Instruments and Methods

Modelling mass balance using photogrammetric and geophysical data: a pilot study at Griesgletscher, Swiss Alps

ANDREAS KÄÄB,[*] MARTIN FUNK

Versuchsanstalt für Wasserbau, Hydrologie und Glaziologie, ETH Zentrum, CH-8092 Zürich, Switzerland

ABSTRACT. The kinematic boundary condition at the glacier surface can be used to give glacier mass balance at a point as a function of changes in the surface elevation, and of the horizontal and vertical velocities. Vertical velocity can in turn be estimated from basal slope, basal ice velocity and surface strain. In a pilot study on the tongue of Griesgletscher, Swiss Alps, the applicability of the relation for modelling area-wide ice flow and mass-balance distribution is tested. The key input of the calculations, i.e. the area-wide surface velocity field, is obtained using a newly developed photogrammetric technique. Ice thickness is derived from radar-echo soundings. Error estimates and comparisons with stake measurements show an average accuracy of approximately $\pm 0.3 \, \text{m a}^{-1}$ for the calculated vertical ice velocity at the surface and $\pm 0.7 \, \text{m a}^{-1}$ for the calculated mass balance. Due to photogrammetric restrictions and model-inherent sensitivities the applied model appeared to be most suitable for determining area-wide mass balance and ice flow on flat-lying ablation areas, but is so far not very well suited for steep ablation areas and most parts of accumulation areas. Nevertheless, the study on Griesgletscher opens a new and promising perspective for the monitoring of spatial and temporal glacier mass-balance variations.

INTRODUCTION

The mass balance at a point of the glacier surface represents the direct climate influence on the glacier at that point. Determining the local mass balance and its distribution pattern on the glacier surface contributes to the monitoring of climate variations and to the understanding and modelling of glacier reaction to climate. Traditional methods of mass-balance determination using stakes and snow pits are time-consuming and expensive, even for a rudimentary network. Just deciding where the "representative" points should be located is in itself a major undertaking. Finally, it would be desirable to obtain mass balance for many glaciers in a geographic region, but this is rarely done because of the tremendous costs involved. Our aim is therefore to devise and test a remote-sensing method of direct mass-balance determination (cf. Haeberli, 1998). In this work, we use photogrammetrically derived velocity fields and a kinematic ice-flow model to determine mass balance over larger areas than is possible with traditional stake measurements.

Direct determination of mass balance by modelling the ice flow is not often done due to the need to specify area-wide boundary conditions at the glacier surface and bed. Rasmussen (1988) obtained both bed topography and mass-balance distribution iteratively, using repeated aero-photogrammetric measurements of elevation and displace-

ments on Columbia Glacier, Alaska, U.S.A. Fastook and others (1995) derived bedrock elevations from repeated aerophotogrammetry. To help analyze an ice core drilled at Dyer Plateau, Antarctica, Raymond and others (1996) calculated the mass balance of the vertical ice column at the drill site. For that purpose, not only the boundary conditions but also a profile of vertical velocity from borehole measurements was used. More often than with the above point-by-point approaches, the discharge fluxes for deriving the mass balance of glacier sections have been calculated. For valley glaciers, longitudinal sections with known average change in elevation and bounded by transverse profiles of velocity measurements are frequently used (e.g. Reynaud and others, 1986). Bindschadler and others (1996) derived the mass balance of ice-stream sections by means of area-wide velocity measurements using a similar approach.

Here we present a method which requires area-wide surface elevation, its changes with time and area-wide surface velocities for input. Glacier bed topography is known from radar measurements. Using these input data and some simple assumptions of ice mechanics, the three-dimensional ice-velocity field at the surface, and subsequently, the mass balance, can be calculated at every point of the glacier surface.

Owing to the size of many alpine glaciers, the resolution of satellite imagery is not adequate to accurately determine surface topography and its temporal three-dimensional variations. Analytical aerophotogrammetry, on the other hand, is a powerful and precise remote-sensing tool for monitoring three-dimensional geometrical changes of gla-

cier surfaces. Nevertheless, its applicability is limited to areas with sufficient optical contrast. Thus, we applied the method described here not on accumulation areas but only on glacier tongues. The promising possibilities as well as the restrictions, the results of ice-flow and mass-balance computation, are shown for the tongue of Griesgletscher, Valais, Swiss Alps, between autumn 1990 and autumn 1991.

SITE DESCRIPTION

Mass-balance measurements on Griesgletscher (Fig. 1) started in 1961. The annual mass balance has been determined using the glaciological method based on a set of stakes. In addition, the photogrammetric method has been applied at intervals of some 5 years, with results that compare well with the glaciological method (Siegenthaler, 1986; Aellen and Funk, 1988; Funk and others, 1997). Bindschadler (1981) simulated the future evolution of Griesgletscher according to different mass-balance assumptions. Hambrey and others (1980) investigated the relation of ice structures and the strain regime. Vieli and others (1997) modelled the three-dimensional ice flow and future behaviour of the whole glacier according to measured and estimated future mass balance. Since 1997, 33 stakes have been drilled over the whole glacier and surveyed several times a year to obtain the surface velocity field. High-resolution aerial photography from a height of about 2000 m above ground (image scale about 1:15 000) is repeated every autumn by the Swiss Federal Office of Cadastral Surveys, covering the entire glacier on one photo strip of about 13 images (Fig. 1).
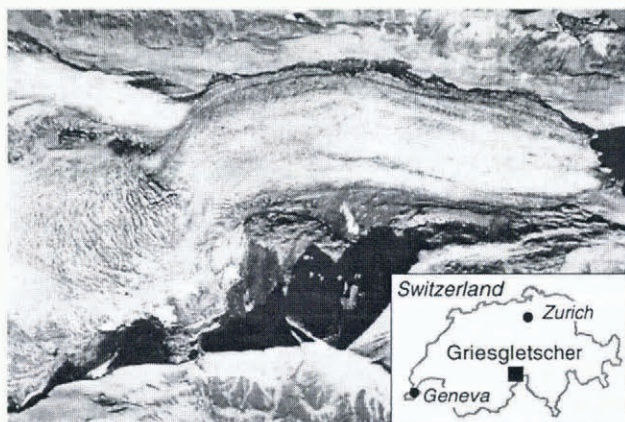

Fig. 1. The tongue of Griesgletscher between the icefall (left) and an artifical reservoir lake (right). Section of an aerial photo taken by the Swiss Federal Office of Cadastral Surveys, 10 September 1991. Griesgletscher is part of the Swiss glacier monitoring network and the object of numerous investigations. Inset: Location of Griesgletscher in the Swiss Alps.

KINEMATIC BOUNDARY CONDITION AT THE GLACIER SURFACE

Basic equations

Our calculations of the local ice flow and mass balance follow the kinematic boundary condition at the surface. In this section we describe the basic equations and the special ice-mechanical assumptions we used for our computation.

From the mass conservation in a vertical column over the entire ice thickness, the local mass balance b at a point (x, y) can be expressed as the difference between the change in surface elevation within time, $\partial z_s / \partial t$, and the horizontal flux differences over ice thickness, $\partial q_x / \partial x$ and $\partial q_v / \partial y$:

$$b(x, y) = \frac{\partial z_s}{\partial t} + \frac{\partial q_x}{\partial x} + \frac{\partial q_y}{\partial y} \qquad (1)$$

(Paterson 1994, p. 256–258). The horizontal flux is the integral of the horizontal velocity components, u and v, over ice thickness, and thus the flux differences can be written as

$$\frac{\partial q_x}{\partial x} = \frac{\partial}{\partial x} \int_{z_b}^{z_s} u \, dz = u_s \frac{\partial z_s}{\partial x} - u_b \frac{\partial z_b}{\partial x} + \int_{z_b}^{z_s} \frac{\partial u}{\partial x} \, dz$$
$$\frac{\partial q_y}{\partial y} = \frac{\partial}{\partial y} \int_{z_b}^{z_s} v \, dz = v_s \frac{\partial z_s}{\partial y} - v_b \frac{\partial z_b}{\partial y} + \int_{z_b}^{z_s} \frac{\partial v}{\partial y} \, dz, \qquad (2)$$

where z_b is the glacier bed elevation, z_s is the surface elevation, u_s and v_s are the horizontal components of surface velocity, u_b and v_b are the horizontal components of basal velocity, $\partial z_s / \partial x$ and $\partial z_s / \partial y$ are the surface slope components and $\partial z_b / \partial x$ and $\partial z_b / \partial y$ are the bed-slope components. Inserting Equation (2) into Equation (1) gives

$$b(x, y) = \frac{\partial z_s}{\partial t} + u_s \frac{\partial z_s}{\partial x} + v_s \frac{\partial z_s}{\partial y} - w_s, \qquad (3)$$

where w_s is the vertical ice velocity at the surface

$$w_s = u_b \frac{\partial z_b}{\partial x} + v_b \frac{\partial z_b}{\partial y} - \int_{z_b}^{z_s} \frac{\partial u}{\partial x} \, dz - \int_{z_b}^{z_s} \frac{\partial v}{\partial y} \, dz. \qquad (4)$$

Equation (4) can be written as

$$w_s = u_b \frac{\partial z_b}{\partial x} + v_b \frac{\partial z_b}{\partial y} - \int_{z_b}^{z_s} \dot{\epsilon}_{xx} \, dz - \int_{z_b}^{z_s} \dot{\epsilon}_{yy} \, dz, \qquad (5)$$

where $\dot{\epsilon}_{xx}$ and $\dot{\epsilon}_{yy}$ are the horizontal strain rates. Assuming incompressibility of ice ($\dot{\epsilon}_{xx} + \dot{\epsilon}_{yy} + \dot{\epsilon}_{zz} = 0$), Equation (5) can be expressed as

$$w_s = u_b \frac{\partial z_b}{\partial x} + v_b \frac{\partial z_b}{\partial y} + \int_{z_b}^{z_s} \dot{\epsilon}_{zz} \, dz, \qquad (6)$$

where $\dot{\epsilon}_{zz}$ is the vertical strain rate. Equations (3) and (6) represent the kinematic boundary condition at the glacier surface (Hutter, 1983; Paterson, 1994). This geometric relation is valid at every point of the glacier surface. Some of the ice-flow components and the connection to geodetic stake measurements and photogrammetric measurements are depicted in Figure 2.

Ice-mechanical assumptions

In our study, we try to determine all the components on the righthand side of Equations (3) and (6) and, subsequently, to calculate the local vertical ice velocity at the surface, w_s, and the local mass balance, b. For that purpose, we use repeated standard photogrammetry to obtain surface slopes and surface elevation changes. A special photogrammetric technique is used to measure surface velocities. Bed topography and ice thickness are derived from ground-based radio-echo soundings. The basal velocity (sliding and sediment deformation) is estimated by comparing an existing ice-flow model for Griesgletscher (Vieli and others, 1997) and measured surface velocities. We obtained a ratio of basal sliding to total surface velocity of about 75% (see below, section on calculated ice flow and mass balance).

To determine the vertical strain at the surface, ϵ_{zz}, it is necessary to know the variations of vertical strain rate with depth. These could be obtained by borehole measurements at single points (e.g. Gudmundsson and others, 1997) or by ice-
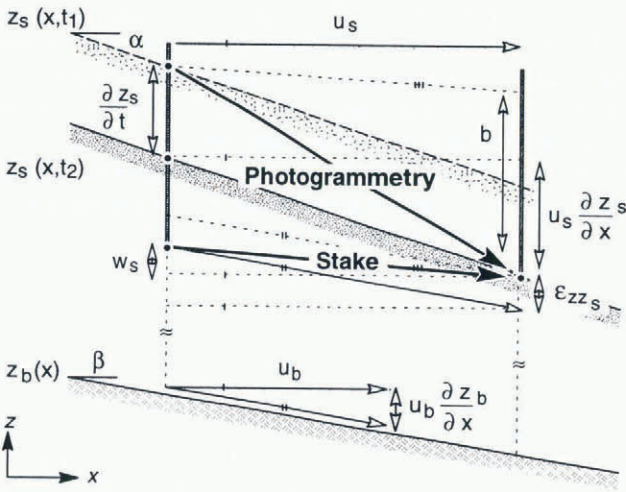
Fig. 2. *Photogrammetric and geodetic measurements and their relation to some components of ice flow, which appear in the kinematic boundary condition at the surface.*

Fig. 3. *Geometry used for determining surface elevation and its changes by monotemporal photogrammetric stereo models and for determining surface displacements by multitemporal stereo models. See text for explanation.*

flow modelling. Gudmundsson and Bauder (1999) give first results of a study on Unteraargletscher, Swiss Alps, which combines the approach using the kinematic boundary condition with a three-dimensional flow model (Gudmundsson, 1997). On Griesgletscher, there are no borehole measurements available, and Vieli and others' (1997) flow model of Griesgletscher does not include sliding, which is assumed to have a marked influence on straining due to the high sliding ratio. Therefore, we decided to estimate the column-averaged vertical strain using the ice thickness, ($h = z_s - z_b$), the vertical strain rate at the surface $\dot{\epsilon}_{zz_s}$ and a simple assumption for the variation of strain rate with depth:

$$\epsilon_{zz_s} = \int_{z_b}^{z_s} \dot{\epsilon}_{zz}\, \mathrm{d}z \approx \gamma h \dot{\epsilon}_{zz_s}. \tag{7}$$

In the case of no internal deformation and pure sliding, γ would be 1 (i.e. vertical strain rate constant with depth). In the case of no sliding, the vertical strain rate at the glacier bed is 0 which, together with the assumption of linear variation of vertical strain rate with depth, gives γ a value of 0.5. As our estimate we use $\gamma \approx 0.75$, considering the high sliding ratio for Griesgletscher tongue, and we introduce a large error estimate for γ in our calculations.

The vertical strain rates at the surface in Equation (7) can be derived from the horizontal ones with $-\dot{\epsilon}_{zz_s} = \dot{\epsilon}_{xx_s} + \dot{\epsilon}_{yy_s}$. The horizontal strain rates at the surface in turn were calculated from the surface velocity field, measured photogrammetrically in our study, using the expression

$$\dot{\epsilon}_{xy} = \frac{1}{2}\left(\frac{\partial v}{\partial x} + \frac{\partial u}{\partial y}\right). \tag{8}$$

SURFACE TOPOGRAPHY AND SURFACE KINEMATICS

Photogrammetric methods

Aerophotogrammetric determination of digital terrain models (DTMs) and subsequent comparison of multitemporal DTMs is an effective and well-established technique for determining glacier surface elevation, surface slopes and the changes in surface elevation. The method uses monotemporal stereo models, composed of at least two overlapping photographs 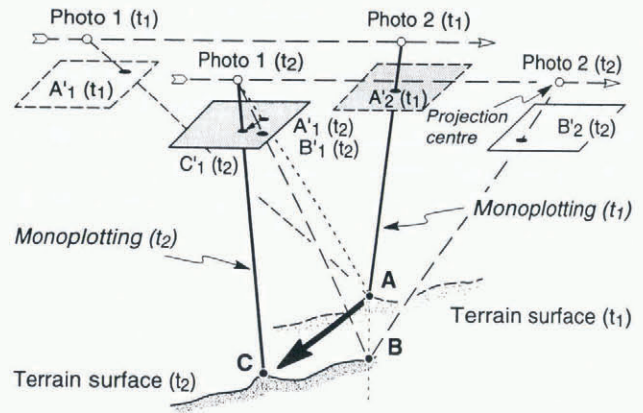taken from different places (spatial baseline). The terrain point A (see Fig. 3) is computed by intersecting two spatial rays, each fixed by the known projection centres and the projections ($A_1'(t_1)$ and $A_2'(t_1)$) of the selected terrain point. Repeating the procedure at other points gives a DTM at time t_1. Repeating the procedure using photographs taken at time t_2 gives the elevation of the same location (point B) and a DTM at time t_2. From both DTMs, the changes in surface elevation throughout the area can be calculated.

To determine surface displacements, a new photogrammetric method to measure surface displacements with high precision was developed and applied, based on the earlier concepts of Flotron (1979), Armenakis (1984) and Saksono (1984). The method was implemented on a computer-aided photogrammetric compilation system (analytical plotter) (Kääb, 1996). It uses multitemporal stereo models composed from aerial photographs taken at different times (temporal baseline) and from different places (spatial baseline) (e.g. photo 1 (t_2) and photo 2 (t_1) in Fig. 3).

Between times t_1 and t_2 the surface point A has moved with the glacier to point C. A marker on the surface or features like closed crevasses or rough ice are suitable targets. The projection of such a point ($A_2'(t_1)$) is chosen on the photo at time t_1. Intersecting the spatial ray fixed by this image point and the known projection centre with the terrain surface, represented by the DTM at time t_1, gives the three-dimensional ground coordinates of point A. This procedure is called monoplotting. The image point $C_1'(t_2)$, which corresponds to $A_2'(t_1)$, can be found using the stereoscopic overlap. The operator cancels the terrain movement between times t_1 and t_2 by displacing one image while simultaneously looking at the multitemporal photographs. This simultaneous and stereoscopic observation supports the identification of corresponding points, improves the accuracy of the measurements and indicates whether a local displacement measurement is consistent with surrounding displacements. In the same way as for the spatial position of point A, the position of point C is computed by monoplotting. Thus, area-wide spatial displacements of the glacier surface can be deduced.

The glacier surface for which the velocity field is determined must show corresponding features in every photograph, and the displacements must be greater than the accuracy of the method. Accuracy increases with the time between the photographs, but the number of corresponding features may decrease. The photogrammetric technique described here

works especially well for analyzing the creep of mountain permafrost (rock glaciers) and is also suitable for observing glacier flow and slope movements (e.g. Gudmundsson and others, 1997; Kääb and others, 1997, 1998; cf. Knizhnikov and others, 1998, for application of a similar technique). It is very difficult to determine displacements on snow-covered terrain, where features are subtle and change rapidly. The accuracy of the method is assumed to be about ±30 μm rms in image scale or, considering the photogrammetric parameters of the Griesgletscher missions, about ±0.4 m rms on the glacier. The accuracy of the displacements was checked by repeating measurements using semi-independent multitemporal stereo models and by comparing the results with geodetic stake measurements on several glaciers and rock glaciers. The comparison for Griesgletscher indicated an accuracy (rms) of the displacement measurements of about ±0.6 m a^{-1} in the case of a 1 year interval between the two photo missions.

Surface elevation

For the photogrammetric measurements two stereo pairs of photographs, taken on 22 August 1990 and 10 September 1991, were used. The orientation was computed from artificial ground markers painted on stable bedrock beside the glacier for which coordinates were known from a geodetic network. DTMs at both times were composed of a regular grid of elevation points with a spacing of 50 m. Each DTM includes about 1000 points on the glacier surface. Contour lines were interpolated from these DTM points and the margin line of the glacier (also determined photogrammetrically) using the DTM interpolation software HIFI (height interpolation using finite elements; Ebner and Reinhardt, 1984). Below the steep icefall, the surface slope of the tongue decreases to a nearly planar middle part at about 2600 m a.s.l., before increasing again towards the terminus (Fig. 4).

Changes in elevation for the period 1990–91 were computed as the difference between the two DTM grids. A Gaussian low-pass filter averaging nine weighted differences to obtain a new smoothed value at the centre point of the 3 × 3 cell filter mask was applied to reduce noise caused by terrain roughness and random measurement errors (Fig. 5). The accuracy of one height measurement is about

Fig. 4. Surface contour lines of the Griesgletscher tongue (in m a.s.l.), derived from a 1990 DTM, and positions of the stakes for determination of mass balance and ice velocity. Coordinates (Swiss system) are in metres.

±0.4 m, so the elevation differences have a standard deviation of about ±0.6 m a^{-1} rms. Over the period 1990–91 the tongue thinned by up to 4 m a^{-1} in the planar middle part (Fig. 5), a considerable thickness loss amounting to about 3% of total ice thickness. During the same year, most other glaciers in the Swiss Alps also experienced significant thinning due to the extremely warm summer. The raw elevation differences outside the glacier margin are at the error level, with some larger amounts caused by (moraine) erosion and melting of ice remains. In Figure 5, depicting the filtered data, the remaining non-zero elevation differences adjacent to the glacier are mostly an artifact of the low-pass filtering, which smooths sharp edges. This can be seen from the fact that the elevation differences decrease to small amounts at greater distances from the glacier. The filtering effect is especially evident at the lake, which despite being at different levels in 1990 and 1991, does not show a uniform change in elevation (Fig. 5).
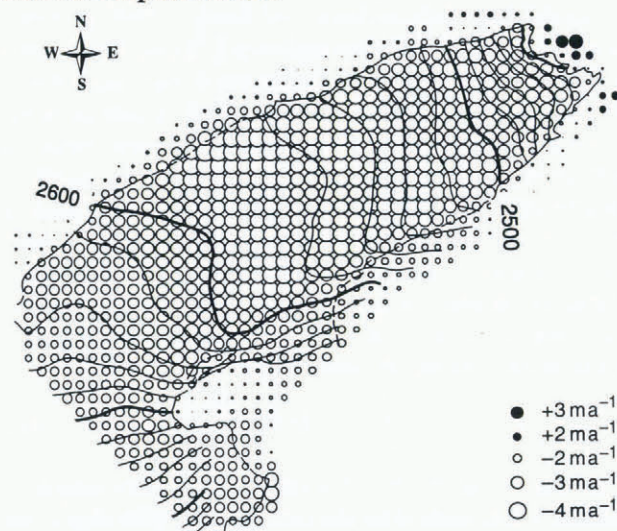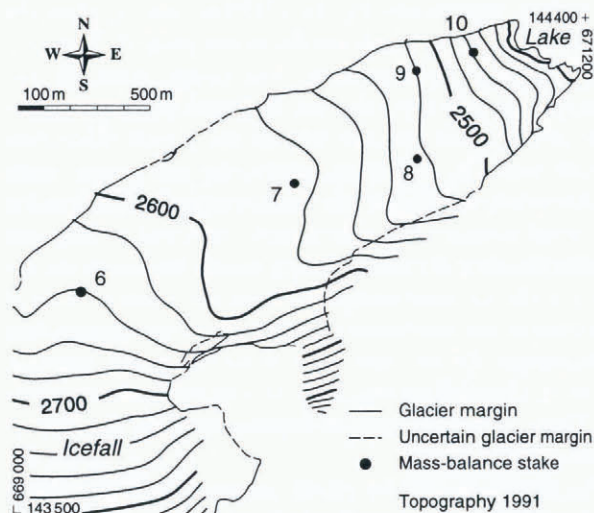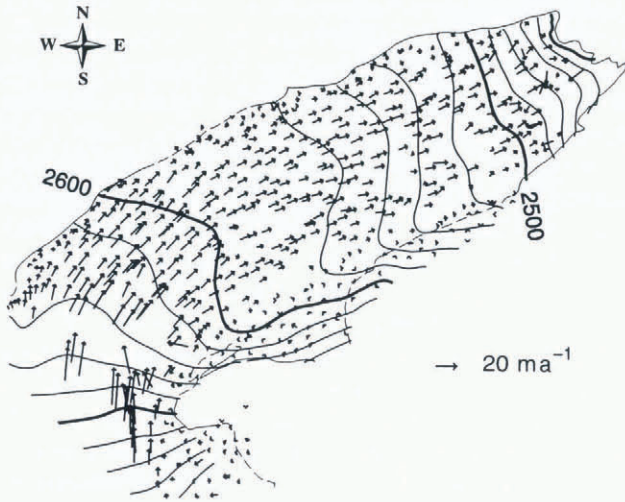
Surface displacements

Fig. 5. Changes in surface elevation on the tongue, 20 August 1990 to 10 September 1991.

The photogrammetric monoplotting technique for determining surface displacements, outlined earlier in this section, was used to derive surface velocities and, subsequently, to calculate surface strain rates and estimate surface strain and basal velocity. Two separate sets of displacements were measured for the period 1990–91, each consisting of about 700 points on the glacier surface. Two multitemporal stereo models were constructed for that purpose, each composed of different photographs of the photo strips of 1990 and 1991 and each newly oriented (i.e. one model of photo 1 (t_2) and photo 2 (t_1), and the other of photo 1 (t_1) and photo 2 (t_2); cf. Fig. 3). The semi-independent sets of displacements help reduce distortion effects in single photographs, errors in the orientation procedures and, most important, errors in single measurements. General error influences, such as bad ground-control points or camera errors, are detected to a lesser extent. Figure 6 shows the raw velocity field obtained from one of the displacement measurement sets. It gives an impression of the basic data quality, while the flow field itself is discussed below (Fig. 7). The velocity vectors in Figure 6 have a density similar to that of the DTMs, i.e. 50 m. Sufficient targets at both times were found in most regions, and measurement was fairly straightforward. In some regions missing targets, low surface

Fig. 6. Raw surface displacement vectors measured by simultaneous monoplotting using a multitemporal photogrammetric stereo model.
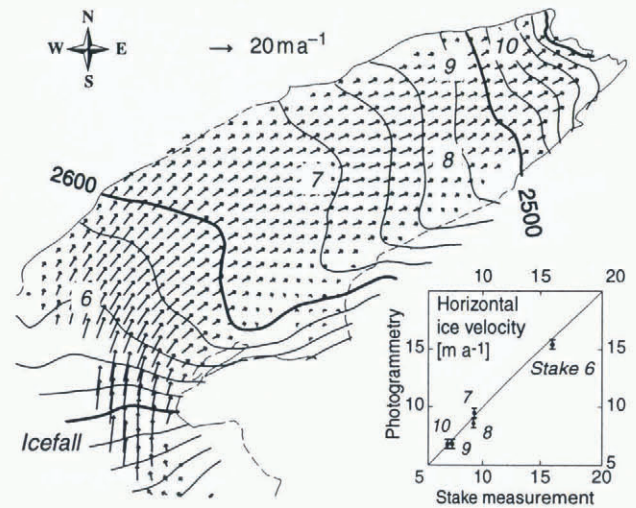

Fig. 7. Surface velocity field of the Griesgletscher tongue during 1990–91, derived from two measurement sets like Figure 6. The results can be compared with surface velocity from stake measurements (inset).

contrast or large surface changes prevented determination of surface displacements. And at a few places, similar but not truly correspondent targets were identified, leading to obvious data blunder.

To compare the two velocity fields, the scattered data were interpolated to a grid with a regular spacing of 50 m using a module of the IMSL mathematical software library (least-square fit to neighbours using quadratic polynomial; Akima, 1978). Extrapolations greater than 50 m from original input data were deleted. Each vector in the first gridded dataset was compared with the corresponding vector in the second set, and a final value was computed as the average of both vectors. Velocities differing >15% in one or more of the two vector components (u, v) in both sets were eliminated, as were velocities measured only in one dataset. The resulting average velocity field was smoothed by the same Gaussian low-pass filter described earlier. After that filtering, data gaps of not more than one gridcell (50 m) were closed by interpolation. The velocity field resulting from this post-processing procedure (Fig. 7) was used for the following calculations. The horizontal velocity accuracy at a single point, deduced by comparison with stake measurements (inset in Fig. 7), was about $\pm 0.6 \, \text{m a}^{-1}$ rms; the accuracy of the average velocity values was about $\pm 0.4 \, \text{m a}^{-1}$ rms.

The highest annual surface velocities during 1990–91 on the Griesgletscher tongue occur in the icefall (up to $40 \, \text{m a}^{-1}$). The surface velocities decrease to $9 \, \text{m a}^{-1}$ in the planar middle part. The photogrammetric results reveal most ice in the ablation area coming from the southern (S) part of the accumulation area. Thus, the flowlines of the northwestern (NW) part of the tongue are shifted against the NW valley flanks. The large ice velocities directly at the NW margin suggests glacier sliding. Below 2550 m a.s.l., ice flow increases to $>10 \, \text{m a}^{-1}$ and then decreases again to $6–7 \, \text{m a}^{-1}$ near the terminus.

Surface strain rates

To model local ice flow and mass balance, we estimate the vertical strain from the vertical strain rate at the surface (cf. Equation (7)). For that purpose, we derive the horizontal strain rates from the surface velocity field using Equation (8). The resulting $\dot{\epsilon}_{xy}$ are sensitive to noise in the raw displacement measurements (cf. Fig. 6), so we apply the smoothed surface velocities (cf. Fig. 7). We use the surface velocity field described in the previous subsection to calculate horizontal strain rates following Nye (1959), in which deformation at a gridpoint is computed from velocities at that point and its four nearest neighbours (see also Bindschadler and others, 1996). Figure 8 shows the horizontal strain rates at the glacier surface transformed to their principal axes. The average strain-rate accuracy, deduced by redundancy in Nye's algorithm, is about $\pm 0.0002 \, \text{a}^{-1}$, only a few per cent of the calculated deformations. The vertical strain rate at the surface (Fig. 9) is derived from the incompressibility condition, $\dot{\epsilon}_{xx} + \dot{\epsilon}_{yy} + \dot{\epsilon}_{zz} = 0$.

The increasing velocities in the upper part of the icefall cause marked extending flow. Strong horizontal compression, and hence vertical extension below the icefall, is due to decelerating flow. As expected, the horizontal strain-rate pattern at the margins (Fig. 8) shows a form and orientation typical for shear deformation. Also, below 2600 m a.s.l. the central glacier experiences very low strain rates as often as longitudinal compression. At 2600–2580 m a.s.l. the ice flow
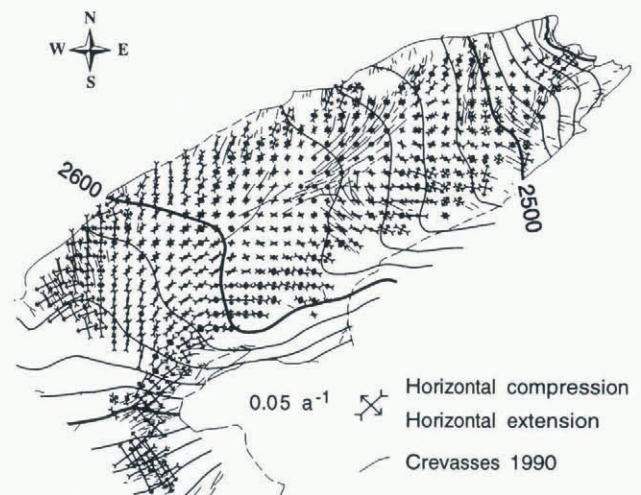

Fig. 8. Horizontal principal surface strain rates during 1990–91 calculated from the velocity field. The crevasses of 1990 were mapped photogrammetrically.
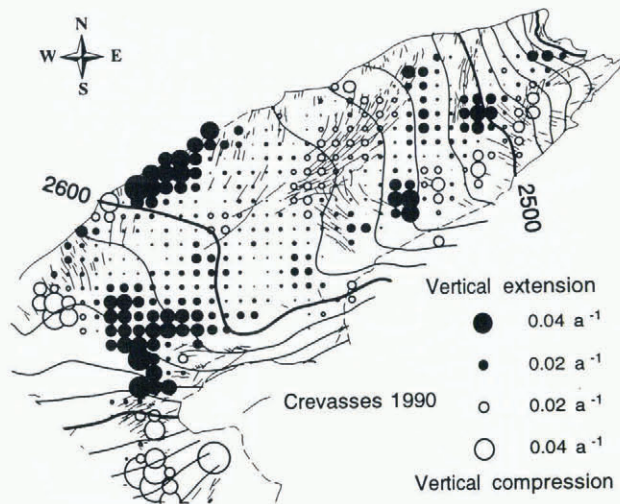
Fig. 9. Vertical surface strain rates during 1990–91 calculated from the horizontal strain rates using the incompressibility condition.

against the NW valley flank causes transverse horizontal compression due to converging flow and, additionally, longitudinal horizontal compression due to decreasing ice velocity. Both together result in strong compression and a rotation of the principal strain-rate axes of about 45° with respect to flow direction. Diverging flow and increasing velocity produce horizontal extension in the middle of the glacier tongue at about 2560–2580 m a.s.l. In most other parts of the tongue, horizontal compression and associated vertical extension predominate, as generally expected for ablation areas.

Figures 8 and 9 also include the 1990 crevasse pattern mapped photogrammetrically. Crevasses are expected where horizontal extension prevails. The orientation of the crevasses should theoretically be perpendicular to the direction of the largest horizontal extension (principal axis) (Vaughan, 1993; Harper and others, 1998). This orientation is consistent for most mapped crevasses on Griesgletscher (Fig. 8; cf. Hambrey and others, 1980). Exceptions may occur, for example, where crevasses advect from regions of horizontal extension into regions of horizontal compression, without having yet totally closed. Small zones of horizontal extension, indicated by crevasse formation but without corresponding evidence in the strain-rate pattern, may have been missed in the strain-rate calculations, possibly due to inadequate resolution of the velocity grid spacing, or to faulty interpolation or excessive smoothing of the velocity field. Finally, the observed pattern of crevasses is the result of some cumulative strain experience prior to 1991, and is not necessarily the result of the strain-rate pattern measured for the period 1990–91.

DETERMINATION OF GLACIER BED TOPOGRAPHY

To estimate the vertical ice velocity at the surface following Equation (6), bed slope and ice thickness have to be known. Both are derived from radio-echo soundings performed in spring 1988 and 1990 along 11 profiles using a monopulse-radar device (Funk and others, 1995). The method used to interpret the data is explained in Fabri (1991). The accuracy of the measurement method as deduced from comparisons of radar-derived ice thickness with deep ice drillings on

several other glaciers is estimated to be about 5–10% of the ice thickness (Haeberli and Fisch, 1984). Additional radio-echo soundings for Griesgletscher are planned, especially in the steep middle part of the glacier where no measurements have been possible so far.

A regular 50 m gridded digital elevation model (DEM) and contour lines (Fig. 10) were interpolated from the ice-thickness profiles using the software HIFI (Ebner and Reinhardt, 1984). The most notable features of the bed topography are the overdeepening between profiles R6 and R9 and the associated transverse bedrock riegel between profiles R9 and R10. This riegel cannot be deduced from the radar measurements alone, and has been inferred from the bedrock topography outside of the glacier. The existence of the interpolated riegel seems to be confirmed by the comparison between modelled ice flow and stake measurements (see following section). Ice thickness of the tongue is up to 150 m in the overdeepening, and about 100 m over the riegel, both relative to the 1991 surface elevation.
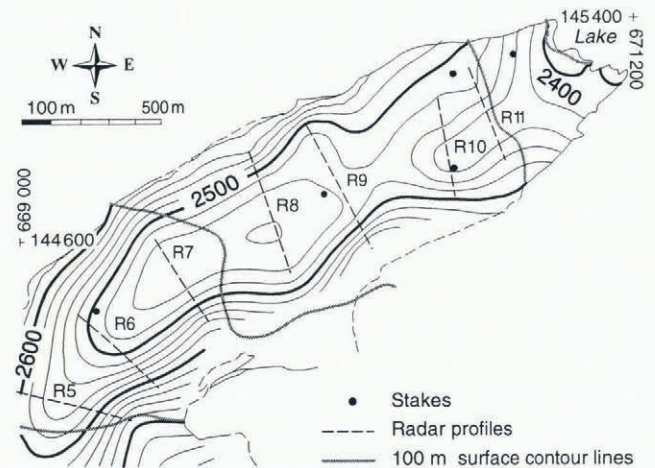

Fig. 10. Glacier bed topography (in m a.s.l.) of the Griesgletscher tongue interpolated from profiles of radio-echo soundings (R5–R11) and bedrock topography of the surrounding ice-free area.

CALCULATED ICE FLOW AND MASS BALANCE

So far we have determined a DTM of the glacier surface, surface velocities and surface strain rates between 1990 and 1991, and a DEM of the glacier bed. To model vertical ice velocity at the surface (w_s) following Equation (6), assumptions for the basal velocity and the relation between the measured surface strain rates and those at depth (cf. Equation (7)) are necessary.

Vieli and others (1997) simulated the ice flow of Griesgletscher using surface and bed elevation data measured by photogrammetry and radio-echo soundings, respectively. Applying a flow model of Blatter (1995), they calculated ice deformation neglecting basal sliding. Comparing the modelled ice deformation at the surface with the velocities measured photogrammetrically gives a ratio of basal sliding to total surface velocity of about 75%. At most places on the glacier tongue the sliding ratio differs by only a few per cent from this value. Deviations in the icefall and at the terminus are artifacts of the flow model's grid spacing (150 m) and of insufficient bed data. Thus, we decided to use the average

Table 1. Approximate average, maximum and error of terms of the kinematic boundary condition at the glacier surface for Griesgletscher tongue (values in flow direction)

Term	Average amount	Maximum amount	Average accuracy
$\partial z_s/\partial t$	$-3\,\mathrm{m\,a}^{-1}$	$-4\,\mathrm{m\,a}^{-1}$	$\pm 0.6\,\mathrm{m\,a}^{-1}$
u_s	$9\,\mathrm{m\,a}^{-1}$	$20\,\mathrm{m\,a}^{-1}$	$\pm 0.4\,\mathrm{m\,a}^{-1}$
$\partial z_s/\partial x$	-0.13	-0.4	± 0.01
sliding/total velocity	0.75	1	± 0.15
$\partial z_b/\partial x$	-0.10	-0.3	± 0.05
$|\dot{\epsilon}_{zz_s}|$	$0.01\,\mathrm{a}^{-1}$	$0.03\,\mathrm{a}^{-1}$	$\pm 0.0002\,\mathrm{a}^{-1}$
h	$80\,\mathrm{m}$	$150\,\mathrm{m}$	$\pm 10\,\mathrm{m}$
assumption for γ (see Equation (7))	0.75	$-$	± 0.25
calculated w_s	$-0.2\,\mathrm{m\,a}^{-1}$	(cf. Fig. 11)	$\pm 0.3\,\mathrm{m\,a}^{-1}$
calculated b	$-4\,\mathrm{m\,a}^{-1}$	$-6\,\mathrm{m\,a}^{-1}$	$\pm 0.7\,\mathrm{m\,a}^{-1}$

Fig. 11. Calculated vertical ice velocity for 1990–91, including comparisons with stake measurements (inset).

sliding ratio of 75% over the whole tongue. The basal velocity is assumed to have the same direction as the surface velocity. For the above approach, we introduce an error of 10–20%. The vertical strain at the glacier surface was estimated from the ice thickness and the vertical strain rate at the glacier surface using Equation (7) and a γ of 0.75, and introducing a large error for this assumption (Table 1).

Using the measured photogrammetric and geophysical data, and the assumptions made above, it is possible to compute the vertical ice velocity at the surface and the local mass balance at every point from Equations (3), (6) and (7). Before describing the results, we discuss the accuracy of the calculations. To analyze the error propagation and the final accuracy of the calculated ice flow and mass balance, we estimate errors for the input data, the ice-mechanical assumptions and the final results (Table 1). To obtain the average accuracy of our model (rms), on the one hand, and to estimate a maximum error range, on the other hand, we take both average and maximum values for the input data, and analyze error propagation for both cases. The resulting maximum model errors are given below in parentheses. For the error analysis we neglect the steep part of the icefall. Slopes and velocities of the estimates are transformed to the flow direction. The errors in bed slope and ice thickness are rough but maximum estimates. Consequently, the error of γ has an effect of up to $\pm 0.2\,\mathrm{m\,a}^{-1}$ (max. 1.1) on the vertical ice velocity, while the error of basal velocity has an effect of only $\pm 0.04\,\mathrm{m\,a}^{-1}$ (max. 0.9). These estimates show that in the special case of the Griesgletscher tongue, the rather rough assumptions for sliding velocity and total vertical strain have a minor effect on w_s due to the low bed slope and low strain rates at the surface (cf. Equation (6)). All errors taken together cause an uncertainty in the calculated vertical ice velocity of about $\pm 0.3\,\mathrm{m\,a}^{-1}$ (max. 1.5), which is dominated by the uncertainty in γ. Errors in elevation change, surface velocity and surface slope contribute an error in the calculated mass balance of $\pm 0.5\,\mathrm{m\,a}^{-1}$ (max. 0.6). Thus, the total error of the mass balance modelled for a point is about $\pm 0.7\,\mathrm{m\,a}^{-1}$ (max. 1.7).

The calculated vertical ice velocity shows some interesting features (Fig. 11). The large negative vertical velocity in the icefall is due to the steep bed slope and is therefore to be expected. The region along the NW margin where the glacier flows towards the NW valley flanks is a conspicuous feature, in which the model calculation yields positive vertical velocities of up to $+3\,\mathrm{m\,a}^{-1}$. This may be due to the ver-
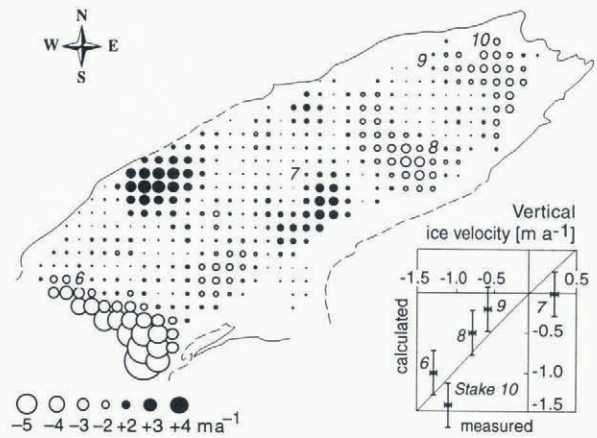
tical strain (cf. Fig. 9). In addition, the flow direction in this area is rotated toward the margin, causing the along-flow bed slope to increase, and hence could result in positive vertical velocities and decreasing horizontal velocities, i.e. compressive flow. Positive vertical velocities at the surface have been calculated upstream of the transverse bedrock riegel, mainly as a result of the increasing bed slope at the riegel. In the remaining parts of the planar middle area the ice flows approximately horizontally, as expected because of the low strain rates and flat bed. At the steeper terminus, below a surface altitude of about 2550 m, it has been calculated that the ice flows downwards in two stages which are the result of bed-slope variations.

Some calculated values of vertical ice velocity can be compared with stake measurements (inset in Fig. 11). The differences show an agreement within the range of the error estimate of $\pm 0.3\,\mathrm{m\,a}^{-1}$. At stake 7, above the transverse riegel, the stake measurement of the vertical velocity confirms the interpolation of this riegel.

Using the vertical surface velocity, the surface slope, the elevation changes and horizontal surface velocity, the distribution of the mass balance for 1990–91 can be calculated (Equations (3), (6) and (7)). The results, plotted on a 100 m grid, are shown in Figure 12. The modelled mass-balance distribution mainly results from the distributions of vertical ice velocity and change in elevation. The glaciological mass-balance measurements at stakes 8–10 agree with calculated values within the error estimate of $\pm 0.7\,\mathrm{m\,a}^{-1}$. At stake 7 no mass balance was available. At stake 6 in the lower part of the icefall, the resulting mass balance does not agree well with the stake measurement, even though the calculated vertical velocity appeared reasonable. Additional photogrammetric measurements were made in this area without detecting any gross errors. The horizontal velocity corresponds well with the stake measurement. Our favoured hypothesis is that this represents a gross error in the stake measurement; however, a difference between modelled and measured mass balance, in principle, may also be caused by the different periods of photogrammetry and stake measurement. The aerial photos used were taken on 22 August 1990 and 10 September 1991, while the stakes were measured on 25 September 1990 and 24 August 1991. Different melting rates in the non-overlapping periods would influence the mass-balance measurement and therefore affect all comparisons between model and field data.

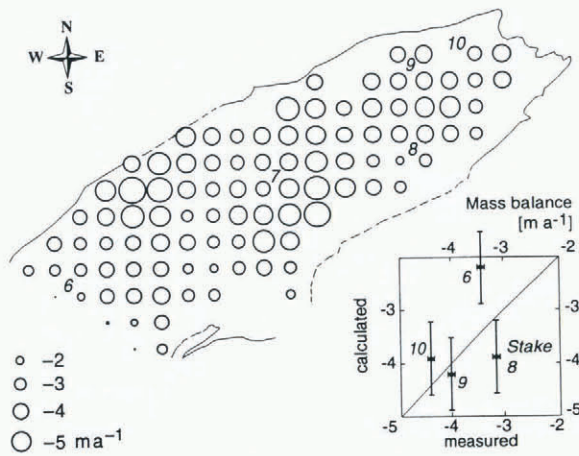Despite the mass balance at stake 7, all differences

Fig. 12. Calculated mass-balance pattern of the Griesgletscher tongue for 1990–91, including comparisons with stake measurements (inset).

between the calculations and the measured vertical ice velocity and mass balance are within the error estimates. Therewith, they are the expected result of the accuracy of the photogrammetric and geophysical methods used, the ice-mechanical assumptions and the error propagation through the kinematic boundary condition.

The modelled mass-balance distribution (Fig. 12) shows a high spatial variability. The values range up to nearly −6 m and vary by a factor of up to 2 at the same altitude. Even taking into account the accuracy of the applied method, these differences remain significant. Several influences may play a role, analysis of which will require further investigations. The obtained mass-balance pattern may be an expression of the solar radiation pattern, the snow distribution and a height gradient of air temperature. The spatial variations of the solar radiation, affecting the snow- and ice melt, depend on the topography of the glacier and of the surrounding terrain. Some low mass-balance values at the SE margin of the glacier may be attributed to the shading of the adjacent mountain ridge, while higher mass-balance values at the NW margin may reflect the absence of such shading. The ice mass-balance pattern is influenced by the snowmelt pattern, and therefore also by the distribution of snow depth over the glacier, which we do not know. The general decrease of mass-balance values to the SW is expected due to the height gradient of air temperature. Enlarged area of the ice surface, and thus high melting rates, may further influence mass balance at zones with crevasses or other high activity such as deformation (e.g. crevasses around stake 7, or strong deformation at the NW margin; cf. Figs 8 and 9).

CONCLUSIONS AND OUTLOOK

The kinematic boundary condition at the glacier surface provides a valuable tool for using area-wide photogrammetrically derived velocity fields and elevation data to model ice flow and mass balance. Ice-mechanical assumptions and data noise can have significant influence on calculated vertical ice velocity and mass-balance values. The effect of errors and assumptions will increase with increasing basal velocity, increasing bed slope and increasing surface slope (cf. Equations (3) and (6)). Therefore, the method is most suitable for planar glacier sections. Additionally, surface strain rates and surface strain can be expected to be low

under such conditions. Applying the model to ice flow over steeper glacier sections like icefalls will be difficult, but, on the other hand, may provide a useful alternative means of determining mass balance for such difficult-to-reach areas.

In addition to these model-inherent restrictions, there are limits imposed by photogrammetric techniques. Photogrammetric determination of elevation and displacement requires sufficient and persistent surface contrast and corresponding features, and is therefore restricted to ablation zones, or to crevassed or rock-covered areas in the accumulation zone. Contrast-giving features on the snow, such as sastrugi or dust, allow for elevation measurement, but often are not persistent enough for displacement measurement. Photogrammetry works much better on contrast-rich debris-covered ice than on the debris-free ice which predominates on Griesgletscher. Therefore, the method described here is especially suitable for determining the mass balance of debris-covered glaciers, which is difficult with other approaches.

To summarise, the modelling of vertical ice flow and mass-balance distribution using area-wide photogrammetric and geophysical data is most promising for ablation areas with low slope (cf. Bauder, 1996; Kääb, 1996). Under the above restrictions, this approach has the potential to reduce the expenditure involved in traditional stake-based mass-balance programmes, for example by helping in siting representative stakes. Finally, this approach provides the spatial variability of the mass balance, which might contribute to improving three-dimensional models of glacier flow, energy-balance models and interpretation of mass-balance processes.

The future goal of modelling glacier mass balance using photogrammetric and geophysical data is to contribute to a remote-sensing strategy for monitoring mass-balance variations. For that purpose, it is necessary to apply repeated annual photogrammetry to obtain a time series of mass-balance distribution. In the case of such time series, the effect of some time-independent errors will be markedly reduced by analyzing only relative mass-balance variations. In fact, first results of a corresponding 20 year series (Kääb, 1996) gave a reasonable mass-balance curve and suggest that even strong errors in glacier bed determination and in the ice-mechanical assumptions were mostly eliminated by calculating differences between annual mass balances.

REFERENCES

Aellen, M. and M. Funk. 1988. Massenbilanz des Griesgletschers von 1961 bis 1986: Vergleich verschiedener Bestimmungsverfahren. *Eidg. Tech. Hochschule, Zürich. Versuchsanst. Wasserbau, Hydrol. Glaziol. Mitt.* 94, 9–50.

Akima, H. 1978. A method of bivariate interpolation and smooth surface fitting for irregularly distributed data points. *ACM Trans. Math. Software,* **4**, 148–159.

Armenakis, C. 1984. Deformation measurements from aerial photographs. *Int. Arch. Photogramm. Remote Sensing,* **25** (A5), 39–48.

Bauder, A. 1996. Massenbilanzmodellierungen mit photogrammetrischen Messungen und eismechanischen Berechnungen am Beispiel des Unteraargletschers. (Diplomarbeit, Eidgenössische Technische Hochschule, Zürich. Versuchsanstalt für Wasserbau, Hydrologie und Glaziologie.)

Bindschadler, R. 1981. The predicted behavior of Griesgletscher, Wallis, Switzerland, and its possible threat to a nearby dam. *Z. Gletscherkd. Glazialgeol.*, **16**(1), 1980, 45–59.

Bindschadler, R., P. Vornberger, D. Blankenship, T. Scambos and R. Jacobel. 1996. Surface velocity and mass balance of Ice Streams D and E, West Antarctica. *J. Glaciol.*, **42**(142), 461–475.

Blatter, H. 1995. Velocity and stress fields in grounded glaciers: a simple algorithm for including deviatoric stress gradients. *J. Glaciol.*, **41**(138), 333–344.

Ebner, H. and W. Reinhardt. 1984. Progressive sampling and DTM interpolation by finite elements. *Bildmess. Luftbildwes.*, **52**, 172–178.

Fabri, K. 1991. Eisdickenmessungen im Aaregletschergebiet, eine Anwendung von Radio-Echo-Sounding. (Praktikumsarbeit, Eidgenössische Technische Hochschule, Zürich. Versuchsanstalt für Wasserbau, Hydrologie und Glaziologie.)

Fastook, J.L., H.H. Brecher and T.J. Hughes. 1995. Derived bedrock elevations, strain rates and stresses from measured surface elevations and velocities: Jakobshavns Isbræ, Greenland. *J. Glaciol.*, **41**(137), 161–173.

Flotron, A. 1979. Verschiebungsmessungen aus Luftbildern. *Eidg. Tech. Hochschule, Zürich. Versuchsanst. Wasserbau, Hydrol. Glaziol. Mitt.* 41, 39–44.

Funk, M., G. H. Gudmundsson and F. Hermann. 1995. Geometry of the glacier bed of the Unteraargletscher, Bernese Alps, Switzerland. *Z. Gletscherkd. Glazialgeol.*, **30**, 1994, 187–194.

Funk, M., R. Morelli and W. Stahel. 1997. Mass balance of Griesgletscher 1961–1994: different methods of determination. *Z. Gletscherkd. Glazialgeol.*, **33**(1), 1996, 41–55.

Gudmundsson, G. H. 1997. Ice deformation at the confluence of two glaciers investigated with conceptual map-plane and flowline models. *J. Glaciol.*, **43**(145), 537–547.

Gudmundsson, G. H. and A. Bauder. In press. Towards an indirect determination of the mass-balance distribution of glaciers using the kinematic boundary condition. *Geogr. Ann.*

Gudmundsson, G. H., A. Iken and M. Funk. 1997. Measurements of ice deformation at the confluence area of Unteraargletscher, Bernese Alps, Switzerland. *J. Glaciol.*, **43**(145), 548–556.

Haeberli, W. 1998. Historical evolution and operational aspects of worldwide glacier monitoring. *In* Haeberli, W., M. Hoelzle and S. Suter, *eds. Into the second century of worldwide glacier monitoring: prospects and strategies.* Paris, UNESCO Publishing, 35–51. (Studies and Reports in Hydrology 56.)

Haeberli, W. and W. Fisch. 1984. Electrical resistivity soundings of glacier beds: a test study on Grubengletscher, Wallis, Swiss Alps. *J. Glaciol.*, **30**(106), 373–376.

Hambrey, M. J., A. G. Milnes and H. Siegenthaler. 1980. Dynamics and structure of Griesgletscher, Switzerland. *J. Glaciol.*, **25**(92), 215–228.

Harper, J.T., N. F. Humphrey and W.T. Pfeffer. 1998. Crevasse patterns and the strain-rate tensor: a high-resolution comparison. *J. Glaciol.*, **44**(146), 68–76.

Hutter, K. 1983. *Theoretical glaciology; material science of ice and the mechanics of glaciers and ice sheets.* Dordrecht, etc., D. Reidel Publishing Co.; Tokyo, Terra Scientific Publishing Co.

Kääb, A. 1996. Photogrammetrische Analyse zur Früherkennung gletscher- und permafrostbedingter Naturgefahren im Hochgebirge. *Eidg. Tech. Hochschule, Zürich. Versuchsanst. Wasserbau, Hydrol. Glaziol. Mitt.* 145.

Kääb, A., W. Haeberli and G. H. Gudmundsson. 1997. Analysing the creep of mountain permafrost using high precision aerial photogrammetry: 25 years of monitoring Gruben rock glacier, Swiss Alps. *Permafrost and Periglacial Processes*, **8**(4), 409–426.

Kääb, A., G. H. Gudmundsson and M. Hoelzle. 1998. Surface deformation of creeping mountain permafrost. Photogrammetric investigations on rock glacier Murtèl, Swiss Alps. *Collection Nordicana* 57, 531–537.

Knizhnikov, Yu. F., R. N. Gelman, G. B. Osipova and D. G. Tsvetkov. 1998. Aerophotogrammetric study of ice movement in surging glaciers. *Z. Gletscherkd. Glazialgeol.*, **34**(1), 69–84.

Nye, J. F. 1959. A method of determining the strain-rate tensor at the surface of a glacier. *J. Glaciol.*, **3**(25), 409–419.

Paterson, W. S. B. 1994. *The physics of glaciers. Third edition.* Oxford, etc., Elsevier.

Rasmussen, L. A. 1988. Bed topography and mass-balance distribution of Columbia Glacier, Alaska, U.S.A., determined from sequential aerial photography. *J. Glaciol.*, **34**(117), 208–216.

Raymond, C., B. Weertman, L. Thompson, E. Mosley-Thompson, D. Peel and B. Mulvaney. 1996. Geometry, motion and mass balance of Dyer Plateau, Antarctica. *J. Glaciol.*, **42**(142), 510–518.

Saksono, T. 1984. Combination of single photographs and digital height models for planimetric and height data extraction. (M.Sc. thesis, The Ohio State University.)

Siegenthaler, H. 1986. Griesgletscher (Wallis) — glaziologische Beobachtungen 1961–1979. *In* Kasser, P., M. Aellen and H. Siegenthaler, *eds. Die Gletscher der Schweizer Alpen 1977/78 und 1978/79. Les variations des glaciers suisses 1977/78 et 1978/79.* Zürich, Gletscherkommission der Schweizerischen Naturforschenden Gesellschaft, 153–180. (Glaziologisches Jahrbuch, Jubilumsband 99 and 100.)

Vaughan, D. G. 1993. Relating the occurrence of crevasses to surface strain rates. *J. Glaciol.*, **39**(132), 255–266.

Vieli, A., M. Funk and H. Blatter. 1997. Griesgletscher: Berechnungen des Gletscherfliessens und Perspektiven für die Zukunft. *Wasser, Energie, Luft — Eau, Énergie, Air*, **89**(5–6), 107–114.